Gelatin-Lysozyme Nanofibrils Electrospun Patches with Improved Mechanical, Antioxidant and Bioresorbability Properties for Myocardial Regeneration Applications

Carvalho, Tiago

2022-05

Carvalho , T , Ezazi , N Z , Correia , A , Vilela , C , Santos , H A & Freire , C S R 2022 , ' Gelatin-Lysozyme Nanofibrils Electrospun Patches with Improved Mechanical, Antioxidant and Bioresorbability Properties for Myocardial Regeneration Applications ' , Advanced Functional Materials , vol. 32 , no. 21 , 2113390 . https://doi.org/10.1002/adfm.202113390

http://hdl.handle.net/10138/351060
https://doi.org/10.1002/adfm.202113390

Additive Manufacturing: Metallurgy, Cut Analysis & Porosity

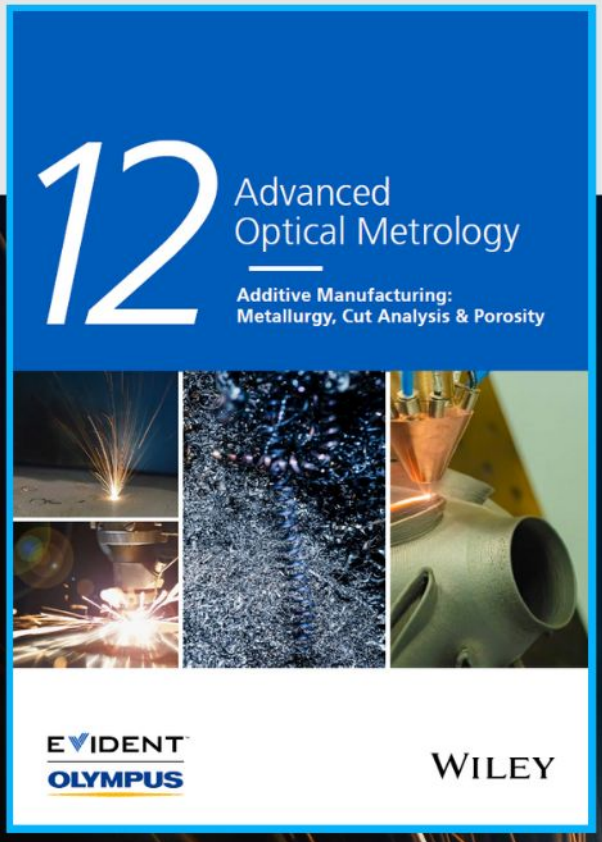

The latest eBook from Advanced Optical Metrology. Download for free.

In industry, sector after sector is moving away from conventional production methods to additive manufacturing, a technology that has been recommended for substantial research investment.

Download the latest eBook to read about the applications, trends, opportunities, and challenges around this process, and how it has been adapted to different industrial sectors.

EVIDENT
OLYMPUS

WILEY

ADVANCED FUNCTIONAL MATERIALS
www.afm-journal.de

Gelatin-Lysozyme Nanofibrils Electrospun Patches with Improved Mechanical, Antioxidant, and Bioresorbability Properties for Myocardial Regeneration Applications

Tiago Carvalho, Nazanin Zanjanizadeh Ezazi, Alexandra Correia, Carla Vilela, Hélder A. Santos, and Carmen S. R. Freire**

Biopolymeric patches show enormous potential for the regeneration of infarcted myocardium tissues. However, most of them usually lack appropriate mechanical performance, stability in water, and important functionalities; for instance, antioxidant activity. Protein nanofibrils, such as lysozyme nanofibrils (LNFs), are biocompatible nanostructures with excellent mechanical performance, water insolubility, and antioxidant activity exploited to fabricate materials for different biomedical applications. In this study, LNFs are used to produce gelatin electrospun nanocomposite cardiac patches with improved properties. The addition of the LNFs to the gelatin electrospun patches enhance their mechanical properties, increasing the patches Young's modulus from 3 to 6 MPa, in their wet state, which agrees with the requirements of myocardial contractility. Additionally, it is observed an increment of the antioxidant activity to 80%, by adding only 5% (w/w) of LNFs, and the bioresorbability rate is shortened to 30–35 d, compared to 45 d for the gelatin-only patches, while maintaining their morphology, and biocompatibility toward cardiomyoblasts and fibroblasts. Furthermore, 15% of a model drug is burst released from the patches and preserved for 21 d. Overall, these results demonstrate that LNFs have a great potential as functional reinforcements to fabricate biopolymeric electrospun patches for myocardial infarcted tissue regeneration.

1. Introduction

According to the World Health Organization, cardiovascular diseases are the leading cause of death in the modern world,[1–3] with myocardial infarction as one of the most prevalent disorders of cardiac tissues.[4,5] After a myocardial infarction, it is difficult for an injured heart to recover because the cardiac muscle tissue lacks for regeneration capacity,[6–8] leading in most cases to heart deformation and failure.[9–11] These are mostly caused by the high oxidative stress,[4,7] the rupture of the extracellular matrix (ECM), and the changes in mechanical performance of the tissue.[3,12] Currently, heart transplantation is still the only effective treatment option,[2,10] and with therapeutic strategies being merely palliative,[10] not resolving the consequences of heart failure,[7,13] thus, alternative strategies are required to reduce the high mortality associated with cardiovascular diseases.[7,9,14] To this end, tissue engineering has been taking advantage of the synergistic relationship between biomaterials, such as biopolymers and living cells, as well as advanced fabrication techniques to prepare functional scaffolds that can promote the regeneration of damaged cardiac tissues.[2,3,6]

There are distinct fabrication techniques that allows the production of fibrous patches, such as electrospinning and spray nebulization.[15–17] Among these techniques, electrospinning is the most widely used one.[18–20] Electrospun structures have several attractive characteristics for biomedical applications, namely the small diameter of the obtained fibers (10 nm to 10 mm), resulting in a high surface area (1–100 $m^2\ g^{-1}$), valuable to cell adhesion, and high porosity (≥80%) and loading capacity and drug encapsulation efficiency (≥90%), which are of vital importance for nutrient diffusion and viability for multifunctionalization, respectively.[21–24] Additionally, electrospun patches can be tailored to better resemble

T. Carvalho, C. Vilela, C. S. R. Freire
CICECO–Aveiro Institute of Materials
Chemistry Department
University of Aveiro
Campus de Santiago, Aveiro 3810-193, Portugal
E-mail: cfreire@ua.pt

The ORCID identification number(s) for the author(s) of this article can be found under https://doi.org/10.1002/adfm.202113390.

DOI: 10.1002/adfm.202113390

T. Carvalho, N. Z. Ezazi, A. Correia, H. A. Santos
Drug Research Program
Division of Pharmaceutical Chemistry and Technology
Faculty of Pharmacy
University of Helsinki
Helsinki FI-00014, Finland
E-mail: h.a.santos@umcg.nl

H. A. Santos
Department of Biomedical Engineering
University Medical Center Groningen/University of Groningen
Ant. Deusinglaan 1, Groningen 9713 AV, The Netherlands

H. A. Santos
W.J. Kolff Institute for Biomedical Engineering and Materials Science
University Medical Center Groningen/University of Groningen
Ant. Deusinglaan 1, Groningen 9713 AV, The Netherlands

the cardiac ECM by aligning the fibers, increasing cardiac cell growth and proliferation.[25–27] Electrospun fibrous patches for the regeneration of infarcted myocardium tissue have been prepared using different polymers,[26,28] among which, biopolymers like gelatin, chitosan, and collagen, have been widely used due to their biocompatibility and bioresorbability.[29,30]

Gelatin, a mixture of peptides resulting from the partial hydrolysis of collagen is widely used for its biological properties to prepare electrospun scaffolds that effortlessly mimic the ECM.[20,31] Indeed, pure gelatin electrospun scaffolds were found to be a good model for long-term culture of myoblasts and cardiomyocytes.[31] However, like most biopolymers, gelatin has inadequate mechanical performance and low stability in water.[30,32] These limitations can be overcome by combining gelatin with synthetic polymers (e.g., polycaprolactone[33] and polyaniline[34]), for the fabrication of implantable bioartificial patches, taking advantage of gelatin properties, while benefiting from the mechanical reinforcement added by the synthetic polymers.[30] More recently, to avoid using synthetic polymers, biopolymeric nanostructures have started to be exploited to strengthen biomaterials prepared integrally from biopolymers, for example, protein-based nanofibrils (NFs).[35,36]

Protein NFs, also known as amyloid fibrils, result from the self-assembly of unfolded proteins and are characterized by a highly organized quaternary structure consisting on conformed β-sheets.[37] These are linked by hydrogen bonds that introduce a rigid internal order to the fibrils.[38] Protein NFs have a typical morphological appearance of bundles of unbranched filaments orthogonally twisted along the axis of each nanofibril.[39] These nanostructures can be formed in vitro, from any protein or peptide.[40] Due to their biological nature and unique features, protein NFs possess remarkable mechanical properties, thermal stability, and insolubility in aqueous media,[41–43] that can be exploited to produce different nanomaterials with improved mechanical properties. For example, Silva et al.[44] prepared pullulan films reinforced with LNFs for food packaging purposes. The incorporation of LNFs also imparted the films with antioxidant and antibacterial activities. The antioxidant activity is a highly desired property for scaffolds for myocardial regeneration due to the increase of reactive oxygen species (ROS) postinfarct.[45] The antibacterial activity is also desired in order to avoid microbial contaminations that might occur during the scaffold's implantation. In a different vein, it has been demonstrated that NFs can act both as nanoreactors and stabilizers to produce gold nanoparticles, particularly to create chain structures of these nanoparticles,[46,47] with functionalities for imaging and electrical conductivity applications.

So far, protein NFs have been explored mostly for biomedical applications, including biosensors, drug delivery systems, bioelectronics, and tissue reparation.[38,48] Regarding regeneration applications, protein NFs have been mainly used for wound healing,[49] spinal cord,[50,51] neural,[52,53] and bone regeneration.[54,55] However, the exploitation of protein fibrils to design innovative biomaterials for myocardium tissue regeneration is still an almost untouched field. Only an implant based on a synthetic elastomeric membrane, a self-assembled peptide hydrogel, and subcutaneous adipose-derived progenitor cells was recently reported for the regeneration of injured myocardium tissue.[56] Thus, this topic deserves further attention as addressed in the present work.

Specifically, LNFs were exploited as functional nanostructures to design electrospun gelatin nanocomposite patches for potential application in myocardial regeneration. Nanocomposite patches with different compositions of gelatin:LNFs were produced and characterized in terms of their morphology, mechanical performance, thermal stability, antioxidant activity, bioresorbability, biocompatibility, and ability to release an incorporated model drug to validate their suitability for the desired application. An optimal patch must recreate the structure, mechanical compliance and microenvironment found on healthy myocardium tissue.

2. Results and Discussion

This work focused on preparing and characterizing innovative electrospun nanocomposite patches based on LNFs as functional nanofillers, and gelatin as the polymeric matrix. LNFs, with a thickness of 34.08±0.01 nm, which is in agreement with the original work,[57] were obtained by fibrillation of lysozyme from hen egg white, using a deep eutectic solvent (DES) (**Figure 1**A). The nanocomposite patches were obtained by electrospinning of suspensions of gelatin with increasing proportions of LNFs (0, 5 and 10% (w/w)) (Figure 1B), followed by crosslinking with glucose through a Maillard reaction.[58] All obtained nanocomposite patches were then characterized in terms of their structure, morphology, mechanical performance, thermal stability, antioxidant activity, bioresorbability, in vitro biocompatibility with rat cardiomyoblast (H9c2) cells and human dermal fibroblasts (HDFs), and their ability to incorporate and release a model drug, curcumin (Figure 1C), to assess the potential for application on the regeneration of infarcted myocardium.

2.1. Structural, Mechanical, Morphological, and Thermal Characterization

First, attenuated total reflectance–Fourier transform infrared (ATR–FTIR) spectroscopic analysis of the electrospun patches was carried out to confirm the crosslinking reaction between the amino groups of both gelatin and LNFs, with the carbonyl group of glucose, promoted by the thermal treatment, typical of Maillard reactions.[58,59] After the thermal treatment, the intensity of the bands at 1080 and 1034 cm^{-1}, associated with C—O vibrations of glucose decreased (**Figure 2**A–C), suggesting that glucose was used during the reaction.[58] Additionally, the band around 3350 nm, associated with the secondary amines N–H stretching decreased considerably for the patch with only gelatin, and gradually less for the samples with 5% of LFNs and 10% of LNFs, suggesting a lower crosslinking extension for the samples containing LNFs.[58] Considering that the total proteic concentration, gelatin along with LNFs, was constant on all three electrospun patches, this event might be explained by the unavailability of the amines contained within the LNFs structure.

SEM imaging was performed on both surfaces (Figure 2D–F) and cross-sections of the electrospun patches (Figure 2G–I). All electrospun fibers are very homogeneous with a smooth surface. Moreover, no agglomerates of LNFs in the patches were visible, suggesting a good dispersion of the LNFs within the

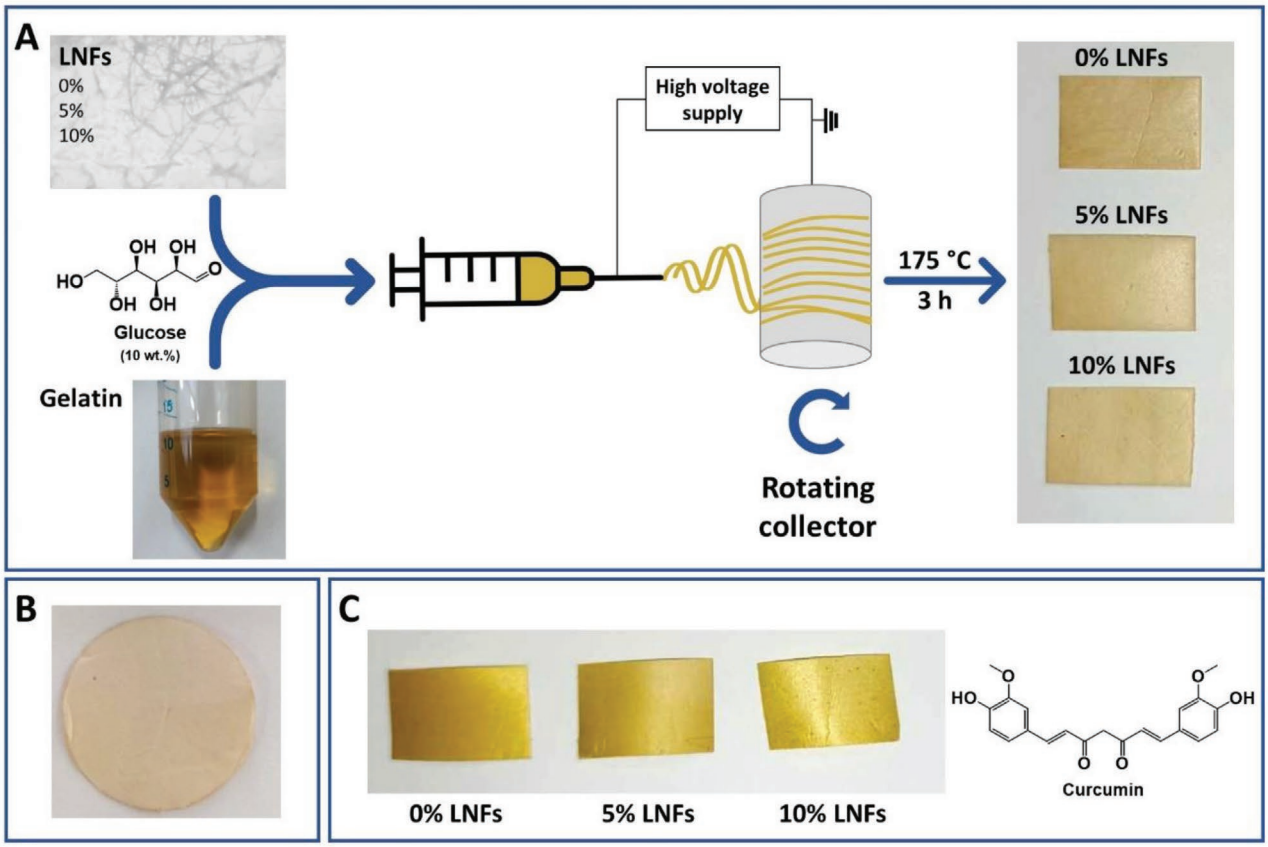

Figure 1. A) Schematic illustration of the fabrication of the electrospun patches of LNFs and gelatin. B) Example of a circular patch cut with a puncher for biological studies. C) Patches containing curcumin used for the drug release studies.

gelatin matrix and a high interfacial compatibility between them. It was also observed that addition of LNFs did not promote statistically relevant changes (one-way analysis of variance (ANOVA)), on the thickness of the electrospun fibers (1.43, 1.70, and 1.79 µm for the patches with 0%, 5%, and 10% of LNFs, respectively), being around 60 times thinner than the ones produced on a previous work on gelatin electrospun fibers preparation (Figure 2M).[58] Although it is not shown, the addition of curcumin to the patches, did not change the fiber morphology and thickness, keeping on having a mean of around 1.5 µm. However, the fiber thickness is dependent on the electrospinning equipment and its setup and surrounding environment. The microscopy images of the cross-section samples revealed the typical formation of layers created by their consecutive collection and deposition.[58] In addition, both the surface and cross-section images of the patches confirm a considerable alignment of the electrospun fibers promoted by their collection using a rotating collector.[60]

The tensile properties of both dry and wet patches, with phosphate buffered saline (PBS), were measured to understand whether they were robust enough to be handled when in the dry state, as well as to assess how they behave after being implanted, thus confirming their well-matched mechanical properties for the myocardium tissue applications. The values of elongation at break, Young's modulus and tensile stress at tensile strength of all samples are shown in Figure 2J–L. Regarding the dry patches, it is noticeable a decrease of the elongation at break, with the increasing proportion of LNFs with statistical differences observed (one-way ANOVA), when comparing with the patches with 0% and 10% of LNFs. Concomitantly, there is a significant increase of the Young's modulus with the increasing amount of LNFs almost reaching 500 MPa for the patch with 10% of LNFs. No significant differences were noticed when comparing the tensile stress at tensile strength of the dry patches with values in the range 0.6–1 MPa. A similar trend was observed for the wet samples, viz. a decrease on the elongation at break with the increasing content of LNFs, from 20 to 12–15% and a steep increase of the Young's modulus from around 3 MPa for the patch with 0% of LNFs to around 6 MPa for both patches containing LNFs. And, once again, no statistical differences (one-way ANOVA), were observed regarding the tensile stress at tensile strength, this time in the range of 0.6–0.8 MPa. These results confirm that the addition of LNFs to the gelatin electrospun fibrous patches promoted an increase on their stiffness, as demonstrated by the rise of the Young's modulus, for both dry and wet samples, and a decrease of elongation at break, reflecting the mechanical reinforcement provided by the LNFs.[44] However, there are observable mechanical differences when comparing the dry and wet patches. The elongation at break increases from values ranging from 2% to 5% to values ranging from 15% to 20%. And the Young's modulus of the patches decreases drastically from 400–500 MPa to 2–6 MPa when wet. The tensile stress at tensile strength of the wet gelatin patches also

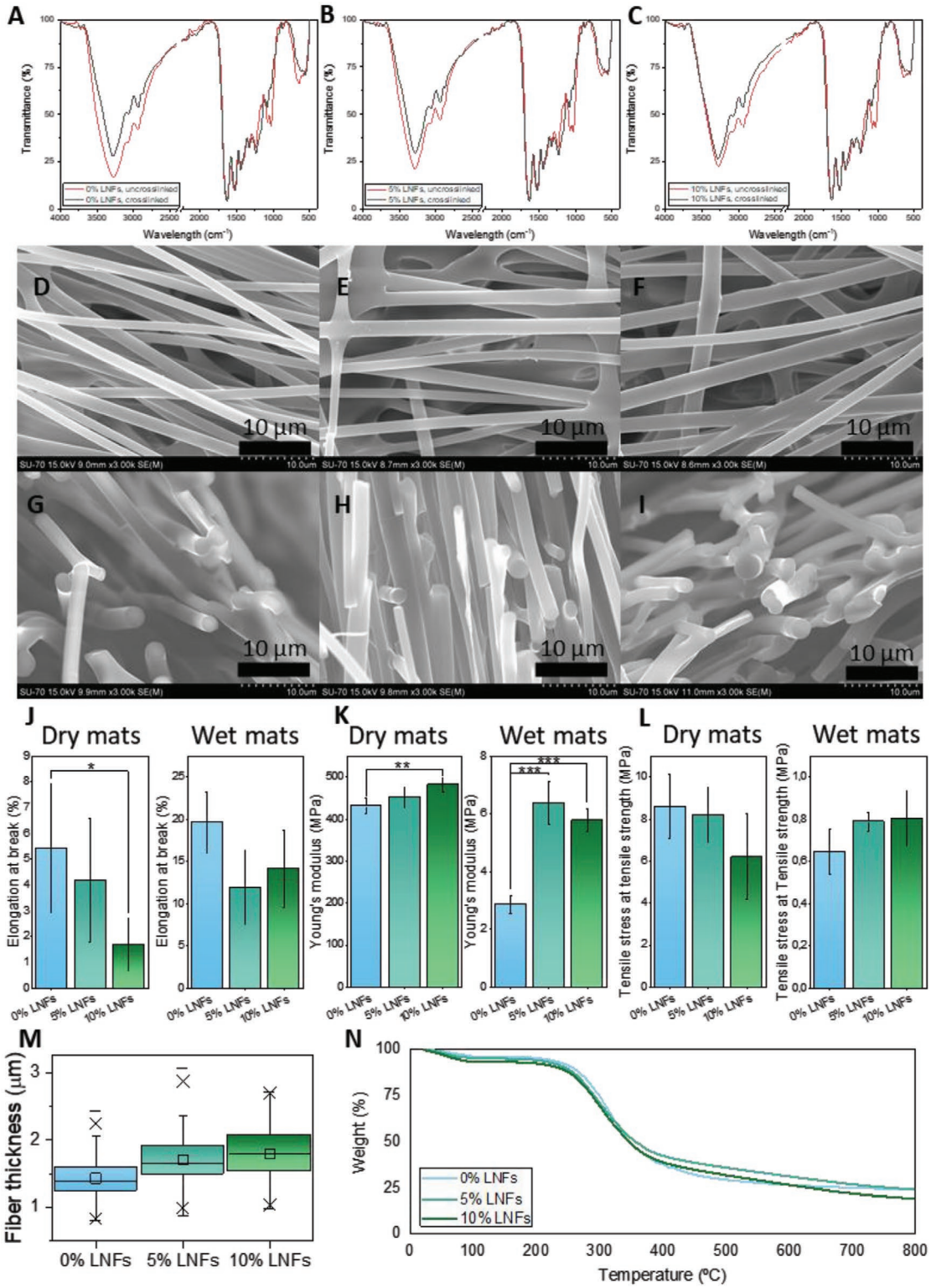

Figure 2. A–C) ATR–FTIR spectra of the electrospun patches (0%, 5%, and 10% of LNFs, respectively), before and after the crosslinking treatment. D–I) SEM microscopy images of the surfaces and cross-sections of the different electrospun patches (0%, 5%, and 10% of LNFs), with a magnification of 3000×. Scale bars are 10 µm. J–L) Graphical display of the tensile assay results, elongation at break (%), Young's modulus (MPa), and tensile stress at tensile strength (MPa) of the dry and wet electrospun patches. The results are expressed as mean ± standard deviations (S.D.). Levels of significance were set at probabilities of $*p < 0.05$, $**p < 0.01$ and $***p < 0.001$, calculated through one-way ANOVA. M) Box-and-whisker plot representing the dispersion of the measured fiber thicknesses ($n = 100$, the boxes and the whiskers represent the quartiles, □ (square) represents the mean value, – represents both minimum and maximum values, and × represents both thresholds between the 1% and 99% values). N) Thermograms of the electrospun patches with different LNFs proportions.

decreases to values ten times lower than the ones measured for the dry patches. This behavior is attributed to the plasticizing effect of water molecules present in the wet patches.[61] Therefore, the mechanical performance of these novel patches is totally in line with the intended application because it is fundamental that in the dry state, they are resistant to deformation, meaning that they are not damaged when being manipulated during their application into the myocardium, while when implanted (in the wet state), will be able to accompany the deformation caused by heartbeats, being within the ideal range considered for myocardial patches, from hundreds kPa to a few MPa.[30] Additionally, these patches showed to have higher Young's modulus on both dry (respectively 40 and 2.5, to 450 MPa, for 0%, 5%, and 10% LNFs samples) and wet states (respectively 0.6 and 0.5, to 6 MPa, for 0%, 5%, and 10% LNFs samples) than poly(glycerol sebacate)-gelatin, and fibrinogen-gelatin electrospun patches,[62] developed for myocardial regeneration. An increase in tensile strength was observed when comparing the patches on their dry states (respectively 2 and 1.2, to 8 MPa, respectively poly(glycerol sebacate)-gelatin, fibrinogen-gelatin, and the gelatin-LNFs patches from the current study). However, a slight decrease was observed when comparing with the wet state of the former patches,[63] (from 1 to 0.8 MPa, respectively poly(glycerol sebacate)-gelatin and the gelatin-LNFs patches from the current study). Nonetheless, compared with the later patches in their wet state,[62] this value is much higher (from 0.01 to 0.8 MPa, respectively fibrinogen-gelatin and the gelatin-LNFs patches from the current study).

Thermogravimetric analysis (TGA) of the three electrospun patches was performed under a nitrogen atmosphere. As can be observed in Figure 2N, all samples displayed a single-step weight loss, with maximum degradation temperatures at around 320 °C for the 0% of LNFs sample and 300 °C for the samples containing LNFs, leaving behind a residue of up to 20–25% of their initial mass at 800 °C. These results indicate that the addition of LNFs slightly decreased the thermal stability of the gelatin patches, possibly due to the lower crosslinking reaction extension as previously discussed,[58] as well as to the slightly lower thermal stability of LNFs that have a single-step degradation profile with a maximum degradation temperature of 308 °C.[44] Nevertheless, all the patches were autoclavable for sterilization at the usual temperature of 250 °C before clinical application.[64]

2.2. Antioxidant Activity

After a cardiac injury, ROS production increases, leading to further damages on the infarcted site.[45,65] A typical form to counter the higher amounts of produced ROS is the use of antioxidants,[45] such as LNFs.[44] In **Figure 3** it is shown the antioxidant activity of the electrospun patches measured by the scavenging of 2,2-diphenyl-1-picrylhydrazyl (DPPH), for 2 h. All patches revealed to have antioxidant activity, peaking after 90 min. After 2 h, the patch without LNFs almost reached an antioxidant activity of 60%, which is usually attributed to some peptides of gelatin from porcine skin with antioxidant activity.[66,67] In addition, both patches containing LNFs had

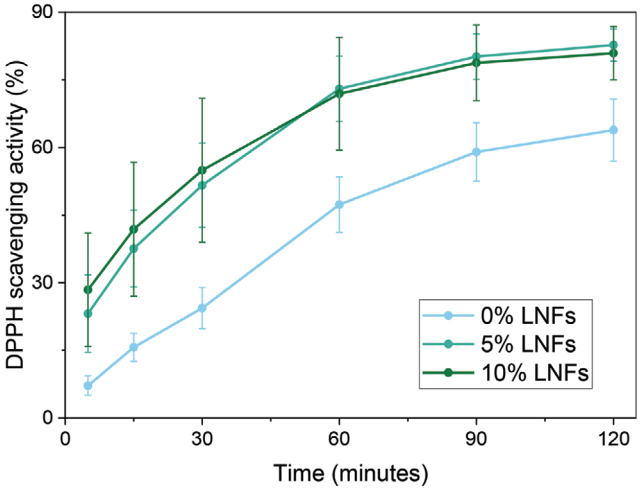

Figure 3. DPPH scavenging activity of the electrospun gelatin patches containing 0%, 5%, and 10% of LNFs. Each point represents the mean of three independent samples. The error bars represent the SD.

similar performances with an antioxidant activity over 20% higher than those of the patch without LNFs, i.e., the addition of a quantity as low as 5% of LNFs on the electrospun gelatin patch was enough to significantly improve the antioxidant activity. Moreover, this activity was observable already at 5 min after incubation with a value of almost 30%. This rapid antioxidant action might help preventing further damage caused by ROS on the infarcted myocardium site.[68] Comparing the antioxidant activity of these patches with that of other electrospun patches for myocardial applications, our results showed to be similar or even slightly better. For example, a ROS-responsive electrospun patch loaded with methylprednisolone was reported to have a DPPH scavenging activity of around 80% after 2 h of incubation,[65] while a core–shell electrospun patch containing ascorbic acid and salvianolic acid B, showed a DPPH scavenging activity of 80% in 30 min;[69] and an oxygen releasing antioxidant polyurethane electrospun patch was reported to have a DPPH scavenging activity of around 80% after 2 h and almost 100% after 5 h of incubation.

2.3. Bioresorbability of the Electrospun Patches and Cytotoxicity of the Degradation Byproducts

In regenerative medicine, one important property of biomaterials is their bioresorbable character, i.e., the biomaterials must be able to degrade at the same rate as the new tissue is formed, and the resulting byproducts must be innocuous for the organism.[70] Thus, the bioresorbability of the gelatin-LNFs electrospun patches was also determined by measuring their mass decrease when incubated in PBS at 37 °C for 45 d. As shown in **Figure 4**A, all electrospun patches were bioresorbable, reaching 25% degradation after 20 d. However, the patches with higher proportions of LNFs, presented a higher bioresorbability rate, with a total degradation after 30 and 35 d for 5% LNFs and 10% LNFs, respectively, compared to 45 d observed for the 0% of LNFs patches. This might be linked with

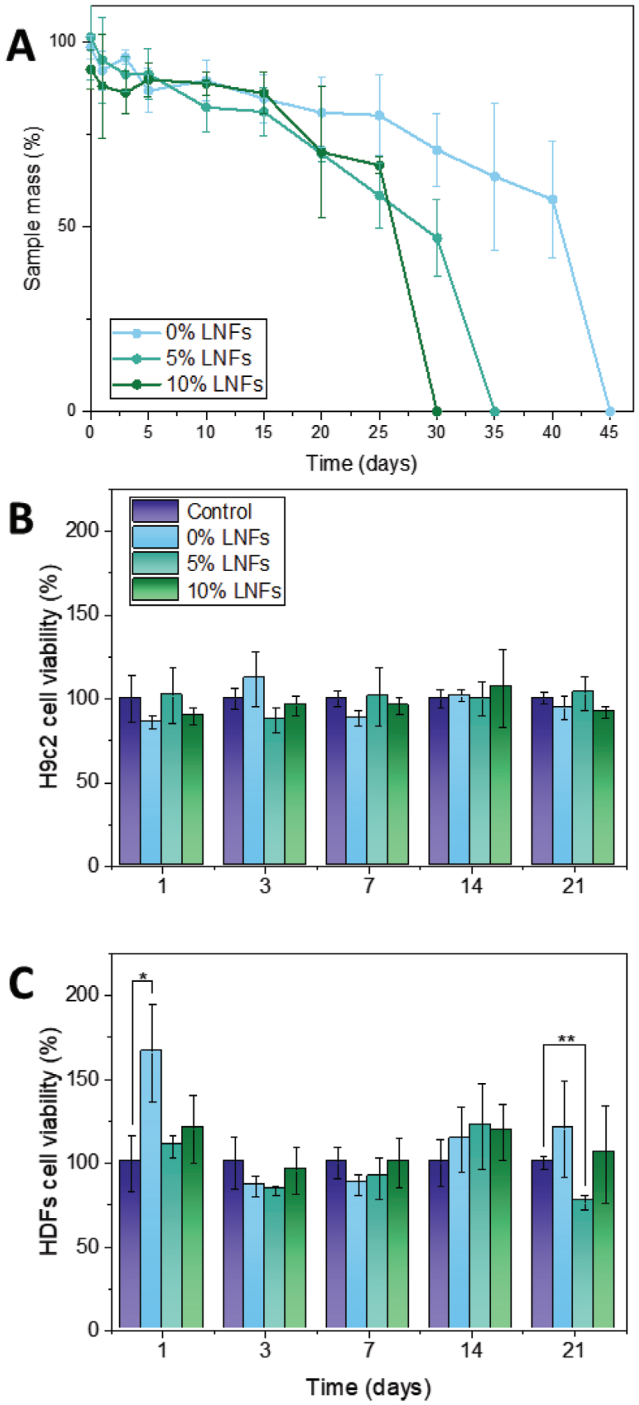

Figure 4. A) Bioresorbability rate of the different electrospun patches calculated by the percentage of mass decrease. The error bars represent the standard deviation ($n \geq 3$). Cell viability of B) H9c2 and C) HDFs cells incubated on the culture media used on the bioresorbability tests with the different electrospun patches (0% LNFs, 5% LNFs, and 10% LNFs), for 1, 3, 7, 14, or 21 d. The results are expressed as mean ± SD. Levels of significance were set at probabilities of $*p < 0.05$, $**p < 0.01$ and $***p < 0.001$, calculated through one-way ANOVA.

a lower crosslinking extension, as shown by the FTIR analysis. Additionally, the mass of all patches was quite stable for at least 20 d (around 75% of the total mass), until it sharply decreased in less than 15 d, suggesting that the patches were steady until reaching a breaking point that leads to a fast degradation ratio, especially with higher contents of LNFs. This is a desired feature, since after having proper cell proliferation, it is required that the implant is degraded, leaving space for a healthy tissue to develop.

Next, to attest that the resulting byproducts of the degradation of each patch were not cytotoxic, a different experiment was carried out. Samples of each patch were infused in culture media for 1, 3, 7, 14, and 21 d, at 37 °C to promote biodegradation. The resulting culture media, containing the degradation byproducts, were then used for model cell culturing in H9c2 cells,[71,72] and HDFs,[24,32] and their viability was measured against cells cultured with normal media after 24 h of incubation. As shown in Figure 4B,C, the viability of the H9c2 cells was not affected by the presence of degradation byproducts of the patches in the culture media, even for the samples after 21 d of degradation, which showed cell viabilities always around 100%. As for HDFs, besides two small discrepancies, on day 1 with the sample containing the degradations byproducts of patch without LNFs that the cell viability increased to around 175% and on day 21 for the sample containing the degradations byproducts of the patch 5% of LNFs that showed a decrease on the cell viability to around 75% the scenario was almost the same as the one observed for the H9c2 cells. In sum, these results confirm that the byproducts that originated during the degradation of all patches are not cytotoxic for the tested cells and under the tested conditions.

2.4. Biocompatibility of the Electrospun Patches

The cytotoxicity of the electrospun patches was evaluated by measuring the cell viability and proliferation of cardiomyoblast H9c2 and HDFs cells, cultured on top of the electrospun patches, for 1, 3, 7, 14, and 21 d, using the CellTiter-Glo assay.[8] Positive (+) control groups were prepared for comparison by cultivating the same cells on wells without the patch, while the negative (−) control groups were prepared on the same fashion as the control (+), but the cells were killed with Triton X-100 a few hours prior to the cell viability measurement. As shown in **Figure 5**, on the first 3 d, for both cell types (H9c2 and HDFs), the cell viability on all electrospun patches was lower than those of the control (+). However, from day 7, it was visible that both cell types were thriving on the electrospun patches, as evidenced by the increase in the cell viability (around 100% or more). For the H9c2 cells, on day 7, there were no statistically significant differences (one-way ANOVA), between the patches and the control (+), while for the HDFs there was a slight increase of the cell viability for the patches to values around 140%. On day 14, the proliferation was much higher (between 225 and 325%) for H9c2 than HDFs (around 100%). These results are very promising, considering the desired application, since H9c2 cells usually do not proliferate as fast as HDFs,[68,73] thus there might be a preferential proliferation of H9c2 cells induced by the patches, which could lead to a better regeneration of the myocardium with a smaller scar formation. On day 21, there was a relative steep decrease of the cell viability of H9c2 proliferation on the patches, and no statistically

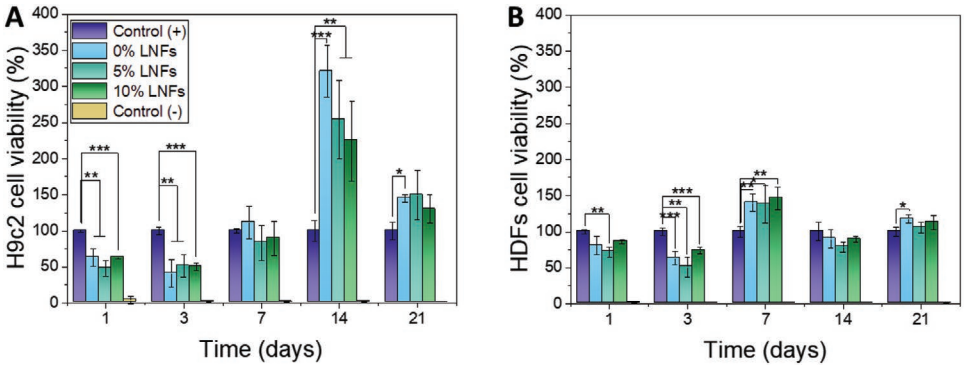

Figure 5. Cell viability and proliferation of A) H9c2 and B) HDFs cells incubated on the electrospun patches for 1, 3, 7, 14, and 21 d. Cells incubated in a well without a patch (control (+)), and cells incubated without a patch and later killed with Triton X-100 (control (−)). The results are expressed as mean ± SD. Levels of significance was set at probabilities of $*p < 0.05$, $**p < 0.01$ and $***p < 0.001$, calculated through one-way ANOVA. Comparing to the controls (−), all samples have a statistically significant difference of cell viability ($***p < 0.001$).

significant differences (one-way ANOVA), were observed with the HDFs cells, indicating that there was no more space in the wells for further cell proliferation, which was further verified with SEM imaging. Furthermore, these results also show that the addition of LNFs to the gelatin electrospun patches did not change their cell viability, which indicates that their quantities can be adjusted to tune the other properties of the patches, such as mechanical performance and bioresorbability ratio, without affecting the cell viability.

Next, the evaluation of the cell attachment was performed for 1, 7, and 21 d by observing the morphology of both cell types when incubated onto the different electrospun patches and a glass slide (used as control) by SEM analysis.[5,71] In **Figure 6**, it is shown the SEM microscopy images displaying the morphology of both types of cultured cells, H9c2 and HDFs. Both cells were thin, elongated, and distended over the three electrospun patches in a similar way between them, but all in better shape than in the control. Cells adhered well to the substrates, confirming the required biocompatibility of the patches for the intended application, supporting the previous cell viability results. As expected, based on the cell viability results, the different patches behaved similarly, with a comparable increase in the number of cells over the substrates throughout the incubation time, and that after 21 d of incubation, all substrates were totally covered by cells. However, the cells cultured on the patches containing LNFs show a higher morphological uniformity, especially visible when comparing the 0% and 10% LNFs samples. Furthermore, another attribute of high value for the described application, is that after 21 d, the patches are fully covered by cells, which considering the beginning of a sharper bioresorbability ratio, as previously discussed, leaves space for the new cells to proliferate and to the formation of the new tissue.

2.5. Drug Loading and Release

Loading implantable scaffolds with drugs to be released on the desired site is very desirable, since it is a shortcut for drug delivery, much simpler than designing a drug that must surpass all natural barriers of the organism to reach the same site.[74–78] In this case, curcumin was used as a model drug because of its anti-inflammatory and cardioprotective properties, that reduce infarct size and ameliorate cardiovascular diseases.[71,79] Curcumin has very low solubility in water, which makes difficult its incorporation into drug delivery vehicles;[80] however, given that the gelatin-LNFs suspensions electrospun were prepared mainly using organic solvents, in this case the incorporation of curcumin was effortless leading to an incorporation of 3.5 mg of curcumin per 80.5 mg patch. As shown in **Figure 7**, on the first day, 15% of the incorporated curcumin was burst-released from all patches, and that quantity was maintained for the duration of the experiment. This phenomenon might be explained by the low solubility of curcumin in aqueous media,[80] which quickly peaked at 15% of the curcumin incorporated into the samples. Nevertheless, the observed bust release of this drug is highly desirable in the first hours postimplantation, and the following constant concentration of curcumin is of additional importance, since curcumin has low bioavailability and is rapidly metabolized,[80] leading to a longer-term therapeutic effect.

During the 3 weeks of the dissolution test, a yellow precipitate (curcumin) was formed in the bottom of the vials that is probably related with the low water solubility of curcumin. In an additional experiment carried out with a solution of curcumin (0.5 mg in 200 mL PBS) incubated in the same way as the patches with curcumin, after 21 d the amount of curcumin in the solution dropped to around 40% of the initial value, and similarly, a deposit of curcumin was also formed in the bottom of the vial. From this experiment we concluded that curcumin is continuously released from the patches granting a constant concentration in solution. In fact, this is in line with the progressive degradation of the patches for this period of time (Figure 4A). To further confirm these results, a 3 d experiment, where each day PBS was changed with a fresh one (Supporting Information) was also carried out. It was observed that, once again, during the first 24 h of incubation, 15% of the incorporated curcumin was released from the patches. On the following days (48 and 72 h), the amount of incorporated curcumin released from the patches was around 3–4%. This way it is confirmed that there is an initial burst release of curcumin from the patches, probably from the most superficially incorporated curcumin, and then, the release continues slowly as the

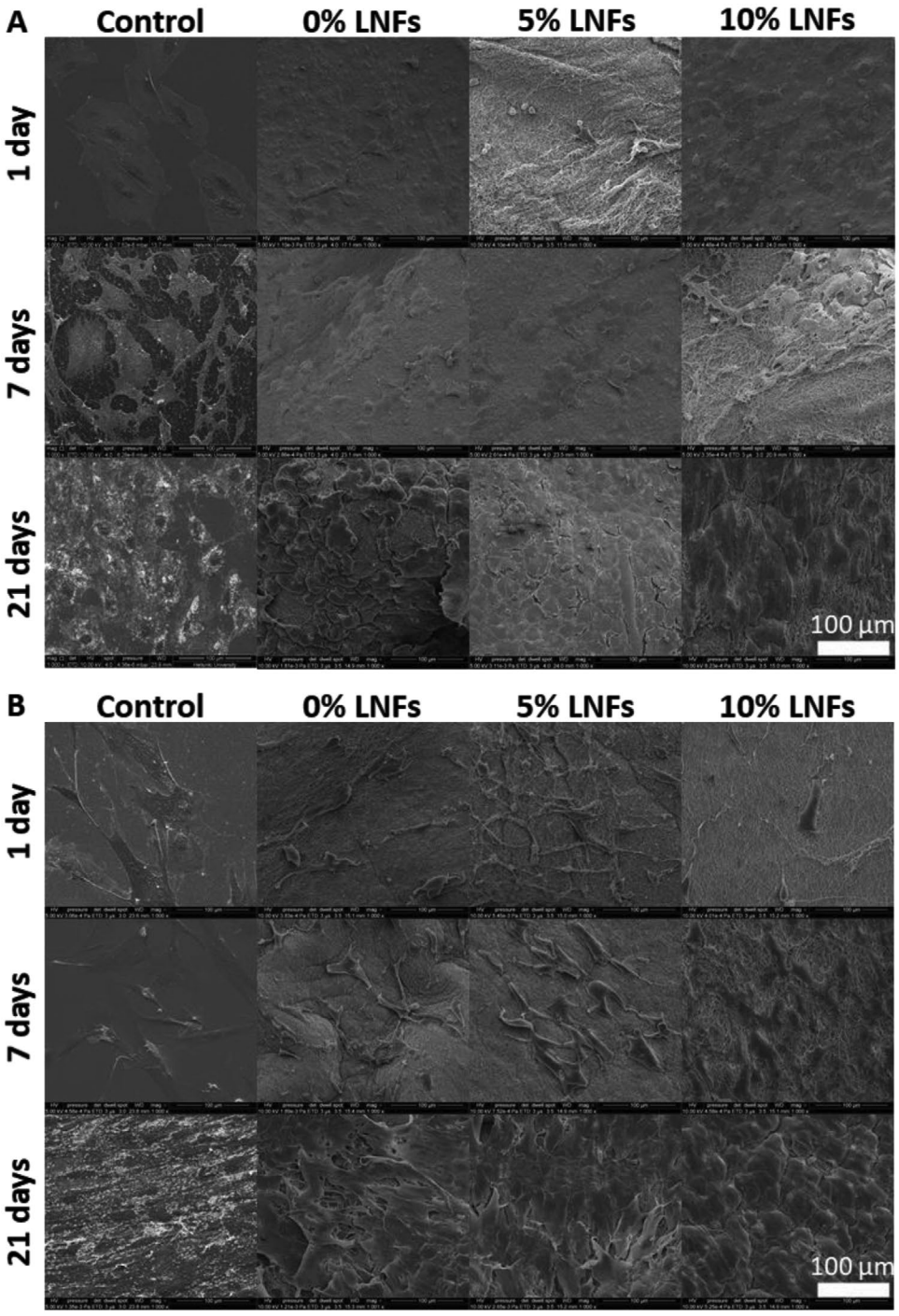

Figure 6. SEM microscopy images of the A) H9c2 and B) HDFs cells after being cultured on the electrospun patches or in a glass slide (control) for 1, 7, and 21 d. Magnification of 1000×. Scale bars are 100 µm.

patches degrade, and the innermost trapped curcumin can be released into the buffer.

Anyway, the amount of released curcumin is similar to the one reported in a previous study, regarding a cardiac patch of nanocellulose, poly(glycerol sebacate) and polypyrrole.[71] Here, we demonstrated that a hydrophobic drug like curcumin can be incorporated within a biopolymeric patch, and be partially burst-released from it, and then maintaining its concentration constant for 21 d, which is the time it took for the patches to be fully covered by cells.

3. Conclusion

In this study, gelatin-LNFs electrospun patches for application in myocardium regeneration were developed. The addition of LNFs

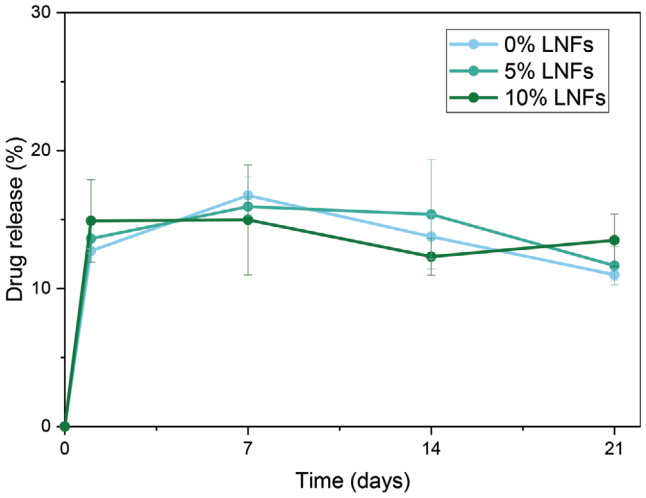

Figure 7. Drug release profiles (%) of the incorporated curcumin during incubation of each electrospun patch on PBS pH 7.4 at 37 °C, with an agitation of 100 RPM. The error bars represent the standard deviation.

to the gelatin patches did not affect the morphology nor the biocompatibility of the electrospun gelatin fibers. Still, it improved their mechanical performance, as seen by the increase of the Young's modulus. Moreover, the addition of LNFs promoted an increment of the antioxidant activity and of the bioresorbability rate (30–35 d compared to 45 d for the patches without LNFs), and partially burst-released (15% in the first day) an incorporated hydrophobic drug, maintaining it at a constant concentration for 21 d. Overall, these results highlight the resourcefulness of LNFs to improve biomaterial patches regarding different properties of interest for myocardial regeneration applications. This study also opens the door for future works on the use of other protein fibers, with distinct functionalities and mechanical properties, as a way to tailor performance of the materials, as well as increase their range of applications.

4. Experimental Section

Chemicals and Cell Lines: 4-(2-hydroxyethyl)-1-piperazineethanesulfonic acid (HEPES, Sigma-Aldrich, USA), Acetic acid (≥99.7%, Sigma-Aldrich, USA), CellTiter-Glo reagent (Promega Corporation, USA), choline chloride (≥98%, Sigma-Aldrich, USA), curcumin (≥95%, ChemCruz, USA), Dulbecco's modified Eagle's medium (DMEM, HyClone, USA), gelatin (Fluka Analytical, UK), D(+)-glucose anhydrous (extra pure, Pharmpur, USP, Spain), glutaraldehyde (25% in H_2O, Merck, Germany), glycine (≥98.5%, Sigma-Aldrich, USA), Hank's Balanced Salt Solution (HBSS, Hyclone, USA), heat inactivated fetal bovine serum (HIFBS, HyClone), hen egg white lysozyme (≈70 000 U mg^{-1}, Sigma-Aldrich, USA), L-glutamine (HyClone SpA, USA), osmium tetroxide (99.95%, Electron Microscopy Sciences, USA), penicillin- streptomycin (PEST, HyClone SpA, USA), PBS (pH 7.4, Sigma-Aldrich, USA), nonessential amino acids (NEAA, HyClone, USA), sodium pyruvate (Gibco, USA), Triton X-100 (Merck, Germany), DPPH (Aldrich, USA). Other chemicals and solvents were of laboratory grades. H9c2 (2–1) were obtained from ATCC CRL1446 (USA), and HDFs cells, were kindly provided by Dr. Christopher Jackson, Mitochondrial Medicine University of Helsinki, Finland.

Preparation of LNFs: LNFs were prepared according to the procedure reported by Silva et al.,[57] with minor modifications. Briefly, 160 mg of lysozyme were placed into a Falcon tube. In another Falcon tube, a DES was prepared by mixing 1.4 g of cholinium chloride and 0.6 mL of acetic acid. Then, 38 mL of a solution prepared with milli-Q water containing 0.2% (v/v) of HCl and 0.15% (w/v) of glycine were added to the Falcon tube containing the DES, and homogenized. Afterward, this solution was used to dissolve the lysozyme, followed by incubation overnight at 70 °C, with stirring. The obtained suspension of LNFs was centrifuged for 45 min at 4 °C and 5000 rpm, and the supernatant was removed. The LNFs were re-suspended in milli-Q water and dialyzed using a dialysis tubing with a cutoff of 10 kDa, for 3 d, changing the outer milli-Q water each 24 h. Finally, the LNFs were frozen, freeze-dried and stored at −20 °C for later use.

Preparation of the Gelatin-LNF Suspensions for Electrospinning: To prepare the suspensions with increasing proportions of LNFs, namely 0%, 5%, and 10% (w/w), distinct quantities of LNFs, 0, 62.5, and 125.0 mg, were added to three different vials, respectively. 125 mg of glucose, and 5 mL of acetic acid 95% (v/v) were also added to each vial. When homogenization was achieved, distinct quantities of gelatin were added to the suspensions on each vial, namely, 1.250, 1.188, and 1.125 g, respectively, meaning that the total polymer concentration was maintained at 25% (w/v). The suspensions were incubated in an orbital shaker at 40 °C, at 300 rpm, until the gelatin was completely dissolved. These proportions of LNFs were chosen to prepare the suspensions, because preliminary experiments showed them to be enough to already observe improvements of the electrospun patches.

Preparation of the Electrospun Patches: All suspensions of Gel-LNFs (25% (w/v)), and a pure gelatin solution (25% (w/v)), were electrospun using an electrospinning apparatus with a rotative collector (10 cm diameter, 6 cm width), covered with an aluminum foil to collect the electrospun fibers. The suspensions were inserted inside a plastic syringe with an inner diameter of 1.3 cm and a syringe needle with an inner diameter of 0.84 mm. The used voltage was 17.0–30.0 kV and the suspension feed was 2.0 mL h^{-1}. The suspension volume used to prepare each patch was 3.0 mL, the distance to the collector was about 10 cm and the rotation speed of the collector was set at 1000 rpm. The obtained electrospun patches were detached from the aluminum foil and put in an oven at 175 °C for 3 h, to promote the crosslinking with glucose through a Maillard reaction.[58] All patches were covered with aluminum foil and stored inside an exicator for posterior use.

ATR–FTIR Spectroscopy: ATR–FTIR spectra of the electrospun patches were obtained on a Perkin Elmer spectrometer (USA) equipped with a single horizontal Golden Gate ATR cell. For each sample 64 scans were recorded between 4000 and 500 cm^{-1}, with a resolution of 2 cm^{-1}, in the absorbance mode.

SEM Imaging: SEM microscopy images of the surface and cross-section of each electrospun sample were obtained using a Hitachi SU-70 microscope (Japan) operating at 15 kV. The cross-section samples were prepared by breaking the patches after immersing them in liquid nitrogen. All samples were previously covered with carbon. Using the image processing software ImageJ, the thickness of the electrospun fibers on each sample was measured.

Tensile Assays: Tensile assays of the electrospun patches were performed using an Instron 5944 (USA) instrument with Bluehill 3 software, using the tensile mode and a 500 N load cell. The samples were cut in accordance with the electrospun fibers orientation, into strips of 50 mm ×10 mm. Specimens of each sample were tested, employing a gauge length of 30 mm. This assay was also carried out for wet patches, previously placed in PBS pH 7.4 until homogeneously wet; In this case, a 50 N load cell and a gauge length of 10 mm was used. The corresponding elongation at break (%), Young's modulus (MPa), and Tensile stress at Tensile strength (MPa) values were plotted. The Young's modulus values were determined from the slope of the low strain region near 0.05%. All results were expressed as the average ±SD ($n \geq 3$).

TGA Analysis: TGA analyses of the electrospun patches were performed using a SETSYS Setaram TGA analyzer (SETARAM Instrumentation, Lyon, France) equipped with a platinum cell. Samples were heated at a constant rate of 10 °C min^{-1}, from room temperature to 800 °C, under a nitrogen flow of 20 mL min^{-1}.

Antioxidant Activity Assessment: The antioxidant activity of the patches was assessed by the DPPH radical scavenging assay.[44] A stock solution

of DPPH was prepared by dissolving 20 mg in 50 mL of methanol. Samples of 5.0 mg, of each patch, were cut and immersed, in triplicates, in vials with 3.75 mL of methanol. A vial containing only 3.75 mL of methanol was used as the control. After adding 0.25 mL of the stock solution on each prepared vial, they were incubated at 37 °C in an orbital shaker at 100 rpm. The absorbance (Abs.) of the samples was measured at 517 nm on a Shimadzu UV-1800 spectrophotometer, at 5, 15, 30, 60, 90, and 120 min, by pipetting aliquots into a quartz cuvette. The antioxidant activity of each sample was calculated according to Equation (1)

$$\text{Antioxidant activity } (\%) = \frac{\text{Abs.}_{\text{control}} - \text{Abs.}_{\text{sample}}}{\text{Abs.}_{\text{control}}} \times 100 \quad (1)$$

Bioresorbability of the Electrospun Patches: For each electrospun patch, specimens with 1 cm^2 were prepared, weighed, and incubated in PBS at 37 °C for different periods of time (0, 1, 3, 5, 10, 15, 20, 25, 30, 35, 40, and 45 d). The PBS buffer was carefully changed every day with a fresh one. For each timepoint, samples were removed from the PBS solution, washed with milli-Q water, frozen, lyophilized and re-weighed to determine the amount of mass lost during the incubation by comparing with the initial mass. At least 3 replicates were done for each sample and time point.

Cell Culturing and Cell Viability: Cell culturing was performed in appropriate well plates, depending on the experiment. The wells to be evaluated were seeded with 5000 cells. Each cell line was incubated with its proper culture media. HDFs cells were incubated with DMEM with 10% (v/v) HIFBS, 1% (w/v) NEAA, 1% (w/v) L-glutamine, penicillin (100 IU mL-1), PEST (100 mg mL^{-1}), and sodium pyruvate. H9c2 cells were incubated with DMEM with 10% (v/v) HIFBS, 1% (w/v) NEAA, 1% (w/v) L-glutamine, penicillin (100 IU mL^{-1}) and PEST (100 mg mL^{-1}). After seeding, each plate was incubated at 37 °C, with an atmosphere of 95% relative humidity and 5% CO_2, until reaching a desired timepoint (1, 3, 7, 14, and 21 d). Afterward, the medium was carefully discarded from each well, and the plate was washed twice with HBSS-HEPES (pH 7.4). Then, 50 µL of CellTiter-Glo and 50 µL of HBSS-HEPES were added to each well. After wrapping the plate with aluminum foil, incubation for 10 min, with mild agitation in an orbital shaker, was carried out. The cell viability was measured with a Varioskan Flash spectral scanning multimode reader (Thermo Fisher Scientific Inc.). The calculations were based on comparisons with the positive control wells, using the correspondent blank wells as background values.

Evaluation of the Cytotoxicity of Degradation Byproducts of the Patches: The cytotoxicity of the byproducts resulting from the degradation of the electrospun patches in culture media, for specific timepoints, was assessed by incubating cells (H9c2 or HDFs cells), in the cell culture media infused with those degradation byproducts. In detail, for each desired timepoint, namely, 1, 3, 7, 14, and 21 d, 5.0 mg of each electrospun patch was placed into Eppendorfs and sterilized in an autoclave. Then, 2.0 mL of culture media for HDFs, were added to each Eppendorf, as well as to empty Eppendorfs, to be used as the controls. After reaching the assigned infusing timepoints (1, 3, 7, 14, and 21 d), in an incubator at 37 °C, the Eppendorfs containing these infused media were collected and frozen at –20 °C for posterior use. After every Eppendorf were collected, 200 µL of each infused culture media was pipetted, in triplicates, into a 96-well plate, and used to cultivate HDFs, and to evaluate the cell viability, as described above. This procedure was repeated for the H9c2 cells, using their correspondent culture medium.

Evaluation of the Cytotoxicity of the Electrospun Patches: To evaluate the cytotoxicity of the electrospun patches toward HDFs and H9c2 cells, the cell viability was accessed for 1, 3, 7, 14, and 21 d. Using a proper puncher, round samples of each electrospun patch were cut (16 mm diameter), perfectly fitting the wells of a 24-well plate. The 24-well plates were prepared by accommodating the punched electrospun patches within the wells: quadruplicate samples to be incubated with cells, as well as the blanks, to be incubated with culture media without cells. In addition, on each plate, 8-wells were left empty, 4 for the negative controls and the other 4 for the positive controls. The punched samples inside the plates, were sterilized with UV irradiation overnight. The HDFs and the H9c2 cells were fed with their correspondent culture media, mimicking the corresponding biological environments. The addition of the culture medium was done slowly and carefully to avoid detachment of the punched samples from the wells. Excluding the blank wells, about 5000 cells were seeded on top of each scaffold, as well as onto the wells of the controls. Cell culturing and viability assessment were performed as previously described.

Cell Attachment: Cell morphology and attachment on the surface of the electrospun patches was investigated using SEM imaging (Hitachi S-4800). The electrospun samples were cut and placed tightly inside 24-well plates, as well as microscope coverslips, as the controls, sterilized overnight under an UV light. The cells (HDFs and H9c2) were seeded on the top of the electrospun samples, as well as on top of the microscope coverslips, and cell culturing followed as previously described. After each timepoint (1, 3, 7, and 21 d), the samples were washed twice with PBS buffer (pH 7.4) and fixed with 2.5% of glutaraldehyde in PBS at 37 °C for 1 h, followed by postfixation, using 1% osmium tetroxide in PBS for 1 h. Afterward, the cells were dehydrated using an increasing gradient of ethanol (50%, 70%, 96%, and 100%). The samples were coated with 5 nm of gold–palladium alloy prior to imaging at 10 kV using a SEM Hitachi S-4800.

Drug Release Studies: For the drug release studies, the electrospun patches were prepared in the same fashion as the ones previously described, with the addition of 62.5 mg of curcumin to each suspension to be electrospun. Each electrospun sample was cut into 80.5 mg pieces, and individually incubated in flasks containing 200 mL of PBS pH 7.4, in an orbital mixer at 37 °C, with an agitation speed of 100 rpm. At each timepoint, an aliquot of 1 mL was collected from each flask and substituted by fresh PBS. Next, 1 mL of ethanol was added to each aliquot, and the absorbance of each one was measured in a spectrophotometer (Shimadzu, Kyoto, Japan), with the wavelength set at 430 nm. The quantity of curcumin measured on each aliquot was calculated through its absorbance against a calibration curve. Afterward, the released quantity of curcumin at a timepoint was calculated using Equation (2), where $m_{\text{curcumin\_aliquots}}$ is the total mass of curcumin removed from the aliquots taken from a flask until the timepoint, C_{measured} is the concentration of curcumin in the aliquot taken on that timepoint, V is the total volume inside the flask, and m_T is the total mass of curcumin loaded into the sample:

$$\%\left(\text{Released curcumin}\right) = \frac{m_{\text{curcumin\_aliquots}} + \left(C_{\text{measured}} \times V\right)}{m_T} \times 100 \quad (2)$$

To evaluate the stability of curcumin in solution, 0.5 mg of curcumin, dissolved in a very small quantity of ethanol, were added to a flask containing 200 mL of PBS (pH 7.4) and incubated during 21 d in the same conditions as previously described for the patches containing curcumin. The amount of curcumin in solution after this period was also determined through its absorbance against a calibration curve.

Statistical Analysis: The results were expressed as mean ± SD of at least three independent sets of measurements. Statistical analysis was done using a one-way ANOVA with the level of significance set at probabilities of $*p < 0.05$, $**p < 0.01$, $***p < 0.001$, analyzed with OriginPro9.0 software (OriginLab Corp.).

Supporting Information

Supporting Information is available from the Wiley Online Library or from the author.

Acknowledgements

This work was developed within the scope of the project CICECO-Aveiro Institute of Materials, UIDB/50011/2020 & UIDP/50011/2020,

financed by national funds through the Foundation for Science and Technology/MCTES. The Portuguese Foundation for Science and Technology (FCT) is also acknowledged for the doctoral grant to T.C. (SFRH/BD/130458/2017) and to the research contracts under Scientific Employment Stimulus to C.V. (CEECIND/00263/2018) and C.S.R.F. (CEECIND/00464/2017). H.A.S. acknowledges financial support from the Sigrid Jusélius Foundation and the Academy of Finland (grant no. 331151). The authors also acknowledge the following core facilities funded by Biocenter Finland: Electron Microscopy Unity of the University for providing the facilities for SEM imaging.

Conflict of Interest

The authors declare no conflict of interest.

Data Availability Statement

The data that support the findings of this study are available from the corresponding author upon reasonable request.

Keywords

electrospun patches, gelatin, lysozyme nanofibrils, myocardium regeneration, nanocomposites

Received: December 30, 2021
Revised: February 4, 2022
Published online: February 27, 2022

[1] M. A. Tölli, M. P. A. Ferreira, S. M. Kinnunen, J. Rysä, E. M. Mäkilä, Z. Szabó, R. E. Serpi, P. J. Ohukainen, M. J. Välimäki, A. M. R. Correia, J. J. Salonen, J. T. Hirvonen, H. J. Ruskoaho, H. A. Santos, *Biomaterials* **2014**, *35*, 8394.
[2] L. A. Reis, L. L. Y. Chiu, N. Feric, L. Fu, M. Radisic, *J. Tissue Eng. Regener. Med.* **2016**, *10*, 11.
[3] N. Zanjanizadeh Ezazi, R. Ajdary, A. Correia, E. Mäkilä, J. Salonen, M. Kemell, J. Hirvonen, O. J. Rojas, H. J. Ruskoaho, H. A. Santos, *ACS Appl. Mater. Interfaces* **2020**, *12*, 6899.
[4] R. Lakshmanan, N. Maulik, *J. Biomed. Mater. Res., Part B* **2018**, *106*, 2072.
[5] M. P. A. Ferreira, S. Ranjan, S. Kinnunen, A. Correia, V. Talman, E. Mäkilä, B. Barrios-Lopez, M. Kemell, V. Balasubramanian, J. Salonen, J. Hirvonen, H. Ruskoaho, A. J. Airaksinen, H. A. Santos, *Small* **2017**, *13*, 1701276.
[6] P.-H. Kim, J.-Y. Cho, *BMB Rep.* **2016**, *49*, 26.
[7] H. Kim, S. H. L. Kim, Y. H. Choi, Y. H. Ahn, N. S. Hwang, *Adv. Exp. Med. Biol.* **2018**, *1064*, 181.
[8] M. P. A. Ferreira, V. Talman, G. Torrieri, D. Liu, G. Marques, K. Moslova, Z. Liu, J. F. Pinto, J. Hirvonen, H. Ruskoaho, H. A. Santos, *Adv. Funct. Mater.* **2018**, *28*, 1705134.
[9] M. P. A. Ferreira, V. Balasubramanian, J. Hirvonen, H. Ruskoaho, H. A. Santos, *Curr. Drug Targets* **2015**, *16*, 1682.
[10] J. Cutts, M. Nikkhah, D. Brafman, *Biomarker Insights* **2015**, *10*, 77.
[11] S. M. Kinnunen, M. Tölli, M. J. Välimäki, E. Gao, Z. Szabo, J. Rysä, M. P. A. Ferreira, P. Ohukainen, R. Serpi, A. Correia, E. Mäkilä, J. Salonen, J. Hirvonen, H. A. Santos, H. Ruskoaho, *Sci. Rep.* **2018**, *8*, 4611.
[12] K. L. Christman, R. J. Lee, *J. Am. Coll. Cardiol.* **2006**, *48*, 907.
[13] B. W. Streeter, M. E. Davis, *Adv. Exp. Med. Biol.* **2019**, *1144*, 1.
[14] G. Torrieri, F. Fontana, P. Figueiredo, Z. Liu, M. P. A. Ferreira, V. Talman, J. P. Martins, M. Fusciello, K. Moslova, T. Teesalu, V. Cerullo, J. Hirvonen, H. Ruskoaho, V. Balasubramanian, H. A. Santos, *Nanoscale* **2020**, *12*, 2350.
[15] Y. Jung, D. Kim, *Biomed. Eng. Lett.* **2021**, *11*, 171.
[16] J. M. Zuidema, T. Kumeria, D. Kim, J. Kang, J. Wang, G. Hollett, X. Zhang, D. S. Roberts, N. Chan, C. Dowling, E. Blanco-Suarez, N. J. Allen, M. H. Tuszynski, M. J. Sailor, *Adv. Mater.* **2018**, *30*, 1706785.
[17] J. Xue, T. Wu, Y. Dai, Y. Xia, *Chem. Rev.* **2019**, *119*, 5298.
[18] M. Kitsara, O. Agbulut, D. Kontziampasis, Y. Chen, P. Menasché, *Acta Biomater.* **2017**, *48*, 20.
[19] F. Topuz, T. Uyar, *Mater. Sci. Eng. C* **2017**, *80*, 371.
[20] S. Babitha, L. Rachita, K. Karthikeyan, E. Shoba, I. Janani, B. Poornima, K. P. Sai, *Int. J. Pharm.* **2017**, *523*, 52.
[21] E. J. Torres-Martinez, J. M. Cornejo Bravo, A. Serrano Medina, G. L. Pérez González, L. J. Villarreal Gómez, *Curr. Drug Delivery* **2018**, *15*, 1360.
[22] N. Bhardwaj, S. C. Kundu, *Biotechnol. Adv.* **2010**, *28*, 325.
[23] M. Qasim, P. Arunkumar, H. M. Powell, M. Khan, *Life Sci.* **2019**, *229*, 233.
[24] Y. Ding, W. Li, F. Zhang, Z. Liu, N. Zanjanizadeh Ezazi, D. Liu, H. A. Santos, *Adv. Funct. Mater.* **2019**, *29*, 1802852.
[25] J. Han, Q. Wu, Y. Xia, M. B. Wagner, C. Xu, *Stem Cell Res.* **2016**, *16*, 740.
[26] G. Zhao, X. Zhang, T. J. Lu, F. Xu, *Adv. Funct. Mater.* **2015**, *25*, 5726.
[27] S. Fleischer, A. Shapira, O. Regev, N. Nseir, E. Zussman, T. Dvir, *Biotechnol. Bioeng.* **2014**, *111*, 1246.
[28] A. K. Capulli, L. A. MacQueen, S. P. Sheehy, K. K. Parker, *Adv. Drug Delivery Rev.* **2016**, *96*, 83.
[29] J. R. Venugopal, M. P. Prabhakaran, S. Mukherjee, R. Ravichandran, K. Dan, S. Ramakrishna, *J. R. Soc., Interface* **2012**, *9*, 1.
[30] V. Guarino, L. Ambrosio, *Electrofluidodynamic Technologies (EFDTs) for Biomaterials and Medical Devices*, Elsevier, Duxford, UK **2018**.
[31] A. Elamparithi, A. M. Punnoose, S. F. D. Paul, S. Kuruvilla, *Int. J. Polym. Mater. Polym. Biomater.* **2017**, *66*, 20.
[32] X. Sun, Q. Lang, H. Zhang, L. Cheng, Y. Zhang, G. Pan, X. Zhao, H. Yang, Y. Zhang, H. A. Santos, W. Cui, *Adv. Funct. Mater.* **2017**, *27*, 1604617.
[33] S. Gautam, A. K. Dinda, N. C. Mishra, *Mater. Sci. Eng. C* **2013**, *33*, 1228.
[34] M. Li, Y. Guo, Y. Wei, A. G. MacDiarmid, P. I. Lelkes, *Biomaterials* **2006**, *27*, 2705.
[35] N. P. Reynolds, *Biointerphases* **2019**, *14*, 040801.
[36] M. Díaz-Caballero, M. R. Fernández, S. Navarro, S. Ventura, *Prion* **2018**, *12*, 266.
[37] A. Portillo, M. Hashemi, Y. Zhang, L. Breydo, V. N. Uversky, Y. L. Lyubchenko, *Biochim. Biophys. Acta, Proteins Proteomics* **2015**, *1854*, 218.
[38] J. Castillo-León, W. E. Svendsen, *Micro and Nanofabrication Using Self-Assembled Biological Nanostructures*, Elsevier, Oxford, UK **2008**.
[39] K. Vus, V. Trusova, G. Gorbenko, R. Sood, P. Kinnunen, *J. Lumin.* **2015**, *159*, 284.
[40] N. Byrne, C. A. Angell, *Chem. Commun.* **2009**, *9*, 1046.
[41] J. E. Gillam, C. E. MacPhee, *J. Phys.: Condens. Matter* **2013**, *25*, 373101.
[42] J. I. Kim, M. Lee, I. Baek, G. Yoon, S. Na, *Phys. Chem. Chem. Phys.* **2014**, *16*, 18493.
[43] B. Choi, G. Yoon, S. W. Lee, K. Eom, *Phys. Chem. Chem. Phys.* **2015**, *17*, 1379.
[44] N. H. C. S. Silva, C. Vilela, A. Almeida, I. M. Marrucho, C. S. R. Freire, *Food Hydrocolloids* **2018**, *77*, 921.
[45] M. Hori, K. Nishida, *Cardiovasc. Res.* **2009**, *81*, 457.
[46] S. Bolisetty, C. S. Boddupalli, S. Handschin, K. Chaitanya, J. Adamcik, Y. Saito, M. G. Manz, R. Mezzenga, *Biomacromolecules* **2014**, *15*, 2793.

[47] D. Lee, Y. J. Choe, Y. S. Choi, G. Bhak, J. Lee, S. R. Paik, *Angew. Chem., Int. Ed.* **2011**, *50*, 1332.
[48] B. He, Y. Ou, S. Chen, W. Zhao, A. Zhou, J. Zhao, H. Li, D. Jiang, Y. Zhu, *Mater. Sci. Eng. C* **2017**, *74*, 451.
[49] N. H. C. S. Silva, P. Garrido-Pascual, C. Moreirinha, A. Almeida, T. Palomares, A. Alonso-Varona, C. Vilela, C. S. R. Freire, *Int. J. Biol. Macromol.* **2020**, *165*, 1198.
[50] M. Sever-Bahcekapili, C. Yilmaz, A. Demirel, M. C. Kilinc, I. Dogan, Y. S. Caglar, M. O. Guler, A. B. Tekinay, *Macromol. Biosci.* **2021**, *21*, 2000234.
[51] H. Liu, X. Xu, Y. Tu, K. Chen, L. Song, J. Zhai, S. Chen, L. Rong, L. Zhou, W. Wu, K. F. So, S. Ramakrishna, L. He, *ACS Appl. Mater. Interfaces* **2020**, *12*, 17207.
[52] X. Fang, C. Zhang, Z. Yu, W. Li, Z. Huang, W. Zhang, *Exp. Neurol.* **2019**, *318*, 258.
[53] C. Schilling, T. Mack, S. Lickfett, S. Sieste, F. S. Ruggeri, T. Sneideris, A. Dutta, T. Bereau, R. Naraghi, D. Sinske, T. P. J. Knowles, C. V. Synatschke, T. Weil, B. Knöll, *Adv. Funct. Mater.* **2019**, *29*, 1809112.
[54] B. He, J. Zhao, Y. Ou, D. Jiang, *Mater. Sci. Eng. C* **2018**, *90*, 728.
[55] G. Wu, M. Pan, X. Wang, J. Wen, S. Cao, Z. Li, Y. Li, C. Qian, Z. Liu, W. Wu, L. Zhu, J. Guo, *Sci. Rep.* **2015**, *5*, 16681.
[56] C. Soler-Botija, J. R. Bagó, A. Llucià-Valldeperas, A. Vallés-Lluch, C. Castells-Sala, C. Martínez-Ramos, T. Fernández-Muiños, J. C. Chachques, M. M. P. Pradas, C. E. Semino, A. Bayes-Genis, *Am. J. Transl. Res.* **2014**, *6*, 291.
[57] N. H. C. S. Silva, R. J. B. Pinto, C. S. R. Freire, I. M. Marrucho, *Colloids Surf., B* **2016**, *147*, 36.
[58] K. Siimon, H. Siimon, M. Järvekülg, *J. Mater. Sci.: Mater. Med.* **2015**, *26*, 37.
[59] L. Deng, Y. Li, F. Feng, H. Zhang, *Food Hydrocolloids* **2019**, *87*, 1.
[60] I. M. El-Sherbiny, M. H. Yacoub, *Global Cardiol. Sci. Pract.* **2013**, *2013*, 38.
[61] Y. I. Matveev, V. Y. Grinberg, V. B. Tolstoguzov, *Food Hydrocolloids* **2000**, *14*, 425.
[62] P. Balasubramanian, M. P. Prabhakaran, D. Kai, S. Ramakrishna, *J. Biomater. Sci. Polym. Ed.* **2013**, *24*, 1660.
[63] M. Kharaziha, M. Nikkhah, S. R. Shin, N. Annabi, N. Masoumi, A. K. Gaharwar, G. Camci-Unal, A. Khademhosseini, *Biomaterials* **2013**, *34*, 6355.
[64] A. Farzan, S. Borandeh, N. Zanjanizadeh Ezazi, S. Lipponen, H. A. Santos, J. Seppälä, *Eur. Polym. J.* **2020**, *139*, 109988.
[65] Y. Yao, J. Ding, Z. Wang, H. Zhang, J. Xie, Y. Wang, L. Hong, Z. Mao, J. Gao, C. Gao, *Biomaterials* **2020**, *232*, 119726.
[66] B. Li, F. Chen, X. Wang, B. Ji, Y. Wu, *Food Chem.* **2007**, *102*, 1135.
[67] O. K. Chang, G. E. Ha, S. G. Jeong, K. H. Seol, M. H. Oh, D. W. Kim, A. Jang, S. H. Kim, B. Y. Park, J. S. Ham, *Korean J. Food Sci. Anim. Resour.* **2013**, *33*, 493.
[68] K. Oyama, K. Takahashi, K. Sakurai, *Biol. Pharm. Bull.* **2011**, *34*, 501.
[69] E. Shoba, R. Lakra, M. S. Kiran, P. S. Korrapati, *Mater. Sci. Eng. C* **2018**, *90*, 131.
[70] S. Saska, L. Pilatti, A. Blay, J. A. Shibli, *Polymers* **2021**, *13*, 563.
[71] R. Ajdary, N. Z. Ezazi, A. Correia, M. Kemell, S. Huan, H. J. Ruskoaho, J. Hirvonen, H. A. Santos, O. J. Rojas, *Adv. Funct. Mater.* **2020**, *30*, 2003440.
[72] M. P. A. Ferreira, S. Ranjan, A. M. R. Correia, E. M. Mäkilä, S. M. Kinnunen, H. Zhang, M. A. Shahbazi, P. V. Almeida, J. J. Salonen, H. J. Ruskoaho, A. J. Airaksinen, J. T. Hirvonen, H. A. Santos, *Biomaterials* **2016**, *94*, 93.
[73] R. F. Brooks, *Nature* **1976**, *260*, 248.
[74] M. Shafiq, Y. Zhang, D. Zhu, Z. Zhao, D.-H. Kim, S. H. Kim, D. Kong, *Regener. Biomater.* **2018**, *5*, 303.
[75] D. Kai, M. P. Prabhakaran, G. Jin, L. Tian, S. Ramakrishna, *J. Tissue Eng. Regener. Med.* **2017**, *11*, 1002.
[76] C. Spadaccio, F. Nappi, F. De Marco, P. Sedati, C. Taffon, A. Nenna, A. Crescenzi, M. Chello, M. Trombetta, I. Gambardella, A. Rainer, *J. Cardiovasc. Transl. Res.* **2017**, *10*, 47.
[77] R. Lakshmanan, P. Kumaraswamy, U. M. Krishnan, S. Sethuraman, *Biomaterials* **2016**, *97*, 176.
[78] H. J. Chung, J. T. Kim, H. J. Kim, H. W. Kyung, P. Katila, J. H. Lee, T. H. Yang, Y. Il Yang, S. J. Lee, *J. Controlled Release* **2015**, *205*, 218.
[79] H. J. Liu, C. H. Wang, Z. Qiao, Y. Xu, *Pharm. Biol.* **2017**, *55*, 1144.
[80] A. Mokhtari-Zaer, N. Marefati, S. L. Atkin, A. E. Butler, A. Sahebkar, *J. Cell. Physiol.* **2018**, *234*, 214.